Study of Li-Al Ferrites by Nuclear Magnetic Resonance, UV-Spectroscopy, and Mossbauer Spectroscopy

J. Mazurenko[1,*], L. Kaykan[2], A. Żywczak[3], V. Kotsyubynsky[4], Kh. Bandura[1], M. Moiseienko[1], A. Vytvytskyi[1]

[1] *Ivano Frankivsk National Medical University, Halytska Str. 2, 76018 Ivano-Frankivsk, Ukraine*
[2] *G.V. Kurdyumov Institute for Metal Physics, N.A.S. of Ukraine, 36 Acad. Vernadsky Blvd., 03142 Kyiv, Ukraine*
[3] *Academic Centre for Materials and Nanotechnology, AGH University of Science and Technology, Krakiw, Poland*
[4] *Vasyl Stefanyk Precarpathian National University, 57, Shevchenko St., 76018 Ivano-Frankivsk, Ukraine*

The paper presents the study of lithium ferrites substituted by aluminum ions by the methods of nuclear magnetic resonance (NMR), Mössbauer spectroscopy, and using a vibrating magnetometer of samples at room temperature. The resulting magnetic moment of the system depends both on the content of the substituting element and on the selective injection into the A or B sublattice. Al^{3+} and Li^+ cations occupy octahedral (B) sites, while Fe^{3+} is distributed in both ones. Implementation of Al^{3+} in the B-position reduces the intensity of the IFNMR echo amplitude. Moreover, an increase in the aluminum content reduces the value of the magnetic superexchange field and causes rapid growth of the paramagnetic component (doublet in Mössbauer spectra). A decrease in saturation magnetization leads to a decrease in signal intensity. Our results showed that NMR and Mössbauer spectroscopy are complementary techniques for describing the magnetic properties of Li-Al ferrites in a wide range of frequencies. Studies of the degradation of methylene blue in an aqueous medium have shown that the synthesized ferrite can act as a photocatalyst operating in the visible light range. It is shown that the optical band gap and the degradation coefficient are inversely related.

Keywords: Li ferrite, NMR, Spinel, Nanocrystalline material, Magnetic Properties, Photo dye-degradation.

1. INTRODUCTION

Substitution of lithium ferrite in the spinel lattice significantly changes the properties of the material [1-6]. So, depending on the type of substitution and the method of synthesis, the magnetic characteristics vary widely. If the non-magnetic substitution element has a strong preference for the octahedral surrounding, then the total magnetization of the system will decrease, and vice versa, when the element is preferred for the tetrahedral surrounding, the substitution by a non-magnetic element leads to an increase in the resulting magnetic moment [7]. Thus, when establishing the effect of substitution on the properties of the synthesized material, special attention is paid to Mössbauer and NMR studies.

Mössbauer's studies of some ferromagnetic spinels [8-10] show that the magnetic fields in the tetrahedral and octahedral sublattices differ from each other by no more than a few tens of kilo Oersted and, thus, give one sextuplet with broadened lines. There is a large amount of experimental data [11-13] in which the experimentally observed spectra are divided into two sextuplets with centroids shifted relative to each other. The splitting of the spectra into two determines the superexchange magnetic fields and their centroids give the isomeric shift in the corresponding sites.

It was shown in works [14-16] that the values of magnetic fields on nuclei are closely related to saturation magnetization, that is, to macroscopic properties. Thus, in this work, we investigate the effect of aluminum ion substitution in cubic lithium spinel on interlattice A-B superexchange interaction. This can be done

based on Mössbauer's studies of the considered sample systems.

The magnetic properties of ferrites largely depend on the distribution of magnetic and non-magnetic cations along the spinel sublattices. Thus, non-magnetic substitutional ions when introduced into the tetrahedral sublattice will strengthen the resulting values of saturation magnetization and vice versa, introducing into the octahedral sublattice and displacing iron ions from there lead to a decrease in magnetization.

The predominant population of cations in these Li-Al ferrite systems was studied using X-ray diffraction (XRD) [17] and Mössbauer spectroscopy. Since the cation distribution [18] determines the magnetic properties of the samples, it is necessary to confirm the distribution of cations by sublattices and the frequency-dependent behavior of the magnetic properties by the method of local samples such as Mössbauer spectroscopy and nuclear magnetic resonance spectroscopy in an external field (IFNMR).

In Ferro/Ferrimagnetic materials, Mössbauer spectroscopy records interlevel transitions (from the ground state $I = 1/2$ to the excited state $I = 3/2$ in the case ^{57}Fe according to the selection rules $\Delta m_I = \pm 1$ and 0) at the resonance of γ-quanta. The energy of γ-quanta changes when the source (or sink) moves according to the Doppler effect [19]. Excited states of ^{57}Fe ($I = 3/2$) nuclei are often associated with an electric quadrupole moment, causing the Zeeman splitting of nuclear excited states. This shift (called a quadrupole nuclear shift of levels) is measured in resonant absorption of γ-quanta. The energy difference

---

* yumazurenko@ifnmu.edu.ua

between the Zeeman splitting of the ground and excited states is a consequence of the interaction of the magnetic fields created by the sample ^{57}Fe nuclei with the nearest magnetic atoms. These magnetic fields are known as magnetic superexchange fields. Magnetic superexchange fields (B_{hf}) are internal fields created by Mössbauer nuclei (in this case by ^{57}Fe). In magnetic materials, these internal fields are sufficient for Zeeman splitting of nuclear levels. This increase in the degeneracy of the ground nuclear state (that is, the state $I = 1/2$ is split $m = + 1/2$ to $m = - 1/2$) is a sign of the presence of ^{57}Fe a magnetic (Ferro/Ferrimagnetic) material. In the one-shot IFNMR method, this splitting as a result of interlevel transitions ($m = + 1/2$ to $m = - 1/2$) in nuclei is carried out using an RF pulse. This energy of interlevel transitions depends on the internal magnetic fields created by the test nucleus ^{57}Fe, but the order of energy is close to the energy of the RF pulse (frequency of the order of MHz). However, in Mössbauer spectroscopy, the transition energy between internal levels (from $I = 1/2$ to $I = 3/2$) is very large (approximately 14.4 keV in the case of ^{57}Fe) and it uses γ-photons.

IFNMR affects local internal fields present in materials. Thus, this method can directly provide information about the possibility of using these materials in high-frequency devices, including radio waves, and micro-waves, since the sampling frequency in NMR is of the order of radio frequencies (RF). Since the observation time is the same as in the case of local studies using a SQUID magnetometer, Mössbauer and NMR spectroscopy are different, these technologies can be used as complementary techniques for a comprehensive analysis of material properties [20]. Moreover, we investigated the magnetic properties of Li-Al ferrite systems using NMR and Mössbauer spectroscopy and supplemented them with magnetic measurements on a vibrating magnetometer of samples VSM 7407. In this work, we showed the possibilities of NMR spectroscopy as one of the important additions to Mössbauer spectroscopy for studying the magnetic properties of ferrimagnetic materials. Since the synthesized materials have a rather small particle size and a large surface area, the possibility of using this finely dispersed ferrite as a photocatalyst for removing impurities from the aqueous medium under visible light irradiation was tested.

2. INVESTIGATION METHODS

Absorption spectra at room temperature from ^{57}Fe were obtained on a Mössbauer spectrometer MS1104EM in the mode of constant accelerations. Cobalt material in a chromium matrix with an activity of 100 mK was used as a source of γ-quanta. Interpreting of the received spectra was carried out in the application package Univem with calibration relative to α-Fe.

Magnetic studies were carried out on a vibrating magnetometer vibration magnetometer 7407 VSM (Lake Shore Cryotronics).

The experimental magnetic moment per m_{exp} formula unit expressed in Bohr magnetons (μ_B) can be calculated using the following formula:

$$m_{exp} = \frac{M_W M_S}{5585}$$

where M_W – molecular weight of the sample and M_S saturation magnetization in emu/g.

The magnetic anisotropy constant (K) can be expressed in terms of the saturation magnetization (M_S) and the magnetic coercive force (H_C) [21] as

$$K = \frac{M_S H_c}{0.96}$$

NMR spectra were recorded on a Bruker Avance III 400 MHz NMR spectrometer.

Optical and degradation studies were carried out on a UV-Vps device (ULAB 108 UV) in the wavelength range of 400-800 nm. For degradation experiments, 0.005 g of methylene blue, 0.15 mg of synthesized ferrite, and 3.5 ml of a 50 % H_2O_2 solution were added to distilled water. After that, the thoroughly mixed mixture was kept in the dark for 40 min to achieve sorption equilibrium. The aged solution, separated from the ferrite component with the help of a permanent magnet, was placed in a spectrophotometer and selected as a zero sample. The rest of the solution was placed under the irradiation of a 150 W halogen lamp. After every 20 minutes, the solution was poured, separated, and the dependence of absorption on the wavelength was obtained. Then the procedure was repeated. Measurements were performed up to 140 minutes of illumination time.

3. RESULTS AND DISCUSSION

3.1 Mössbauer Studies

Experimental Mössbauer spectra of aluminum-substituted lithium spinel synthesized by the sol-gel autocombustion method are shown in Fig. 1.
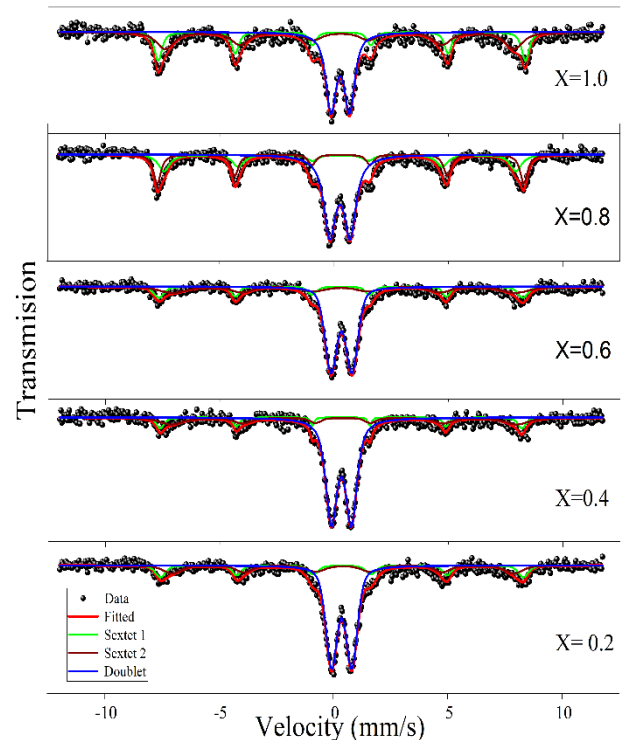

Fig. 1 – RT Mössbauer spectra of Li$_{0.5}$Al$_x$Fe$_{2.5-x}$O$_4$ (x = 0.2, 0.4, 0.6, 0.8, 1.0)

Mössbauer spectra are characterized by a well-defined paramagnetic doublet that coexists with a magnetically ordered component. In Fig. 1, what corresponds to $Li_{0.5}Fe_{2.5}O_4$ (substitution $x = 0.0$) two sextuplets corresponding to two sublattices are observed. The values of the magnetic fields in the tetrahedral and octahedral positions are 499 and 512 kOe, respectively. In Fig. 1 ($x = 0.4$ to $x = 1.0$), we found that in addition to the sextuplet, a doublet appears in the center, the intensity of which increases with increasing aluminum content. The centroids of the magnetic and quadrupole spectra are shifted relative to each other, the latter being more negative by approximately 0.13 mm/s. The splitting of the doublet, as it turned out, is almost independent of the aluminum content. At room temperature, the total value of the magnetic field in aluminum-substituted compounds does not decrease monotonically with increasing aluminum content, as might be expected from the large changes in their Néel temperature TN.

The value of the magnetic fields turned out to be of the same order of magnitude and equal to (487 ± 7) kE.

The occurrence of a doublet together with sextuplets can be explained as follows. The direction of exchange or superexchange interaction with magnetic neighbors is responsible for magnetic ordering. In the studied system, the replacement of magnetic atoms involved in the exchange interaction with a given iron atom by non-magnetic ions Al3+ isolates some iron atoms from other magnetic ions of the lattice participating in the magnetic interaction. An isolated sample ion should relax relatively faster while introducing an additional iron ion into the number of neighbors of the ion under consideration increases the relaxation time. In some works, on Mössbauer's research [22-26], a similar effect is attributed to the so-called phenomenon of superparamagnetism. Mössbauer spectra of superparamagnetic systems are similar to paramagnetic systems due to relaxation effects.

Table 1 – Parameters of the components of Mössbauer spectra of system 1

Degree of substitution x		Parameters of partial schedule components					
		Isomer shift IS, mm/s				Isomer shift IS, mm/s	
0.2	sextuplet (B)	0.3336	0.2		sextuplet (B)	0.3336	0.2
	sextuplet (A)	0.383			sextuplet (A)	0.383	
	doublet	0.322			doublet	0.322	
0.4	sextuplet (B)	0.299	0.4		sextuplet (B)	0.299	0.4
	sextuplet (A)	0.398			sextuplet (A)	0.398	
	doublet	0.311			doublet	0.311	
0.6	sextuplet (B)	0.289	0.6		sextuplet (B)	0.289	0.6
	sextuplet (A)	0.360			sextuplet (A)	0.360	
	doublet	0.313			doublet	0.313	
0.8	sextuplet (B)	0.315	0.8		sextuplet (B)	0.315	0.8
	sextuplet (A)	0.286			sextuplet (A)	0.286	
	doublet	0.278			doublet	0.278	
1.0	sextuplet (B)	0.327	1.0		sextuplet (B)	0.327	1.0
	sextuplet (A)	0.262			sextuplet (A)	0.262	
	doublet (B)	0.262			doublet (B)	0.262	
Errors		±0.001	Errors			±0.001	Errors

Fig. 2 shows the Al NMR spectra for all the studied samples. The general formula for the frequency in NMR is given by equation [27].

$$f = \frac{\gamma H_{if}}{2\pi},\qquad(1)$$

where f is resonance frequency (MHz), γ is a gyromagnetic ratio of the active NMR nucleus (Hz/T), and H_{if} is an internal magnetic field (superexchange field resulting from various magnetic interactions, including Fermi-contact interaction and similar) (T).

According to equation (1) and given NMR results, it can be noted that Al^{3+} ions occupy two different positions. Moreover, the peak corresponding to the octaposition remains much more intense than the others for all the studied samples. This indicates that aluminum ions in ferrite spinel occupy mainly octahedral positions. Although with relatively large substitutions, some of the ions move into tetrapositions, which is indicated by the peaks in the spectra. A strongly separated and shifted peak in the region of higher frequencies on the sample with $x = 1.0$ indicates that part of the aluminum ions falls into a separate phase.

As can be seen from the figure, the position of the resonance lines shifts towards higher field values, and the height increases for substitutions ($x = 0.4$ and 1.0) and decreases for substitutions $x = 0.6$ and 0.8. In addition, for large substitutions ($x = 0.8$ and 1.0) in the region of large fields, an additional influx is observed. This may be a sign that some of the aluminum ions fall into a separate phase, which is also confirmed by NMR studies [28-30].

3.2 Magnetic Properties

M-H loops for all samples were obtained at a maximum field of 10000 E at room temperature in two modes: before and after heating to a temperature of 900 K, as shown in Fig. 4. It was found that the saturation magnetization changes non-monotonically for samples with aluminum content from $x = 0.2$ to $x = 0.8$, at which the magnetic characteristics acquire
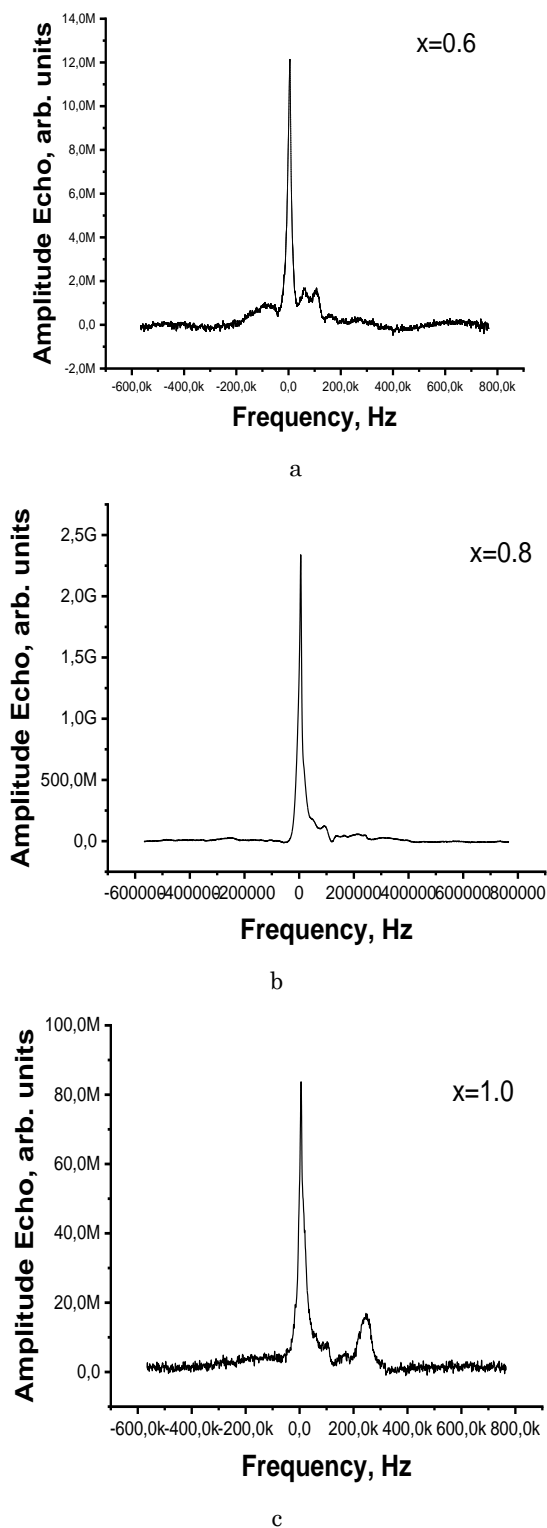
a

b

c

Fig. 2 – The ^{57}Fe IFNMR spectra on lithium ferrite with the substitution of non-magnetic Aluminum cations. The NMR spectra shown for samples $Li_{0.5}Al_xFe_{2.5-x}O_4$, ($x = 0.6$ (a); 0.8 (b); 1.0 (c))

the greatest value, but at $x = 1.0$, their sudden decrease is observed. This behavior can be explained based on Neel's two-sublattice model [31, 32]. It is known that lithium ferrites are inverse spinels, in which Li^+ and Fe^{3+} ions occupy octahedral (B) positions in the ratio 1:3 and tetrahedral (A) positions are filled only with Fe^{3+} ions $[Fe_1^{3+}]_A[Li_{0.5}^{1+}Fe_{1.5}^{3+}]_BO_4$. In aluminum-

substituted ferrites $Li_{0.5}Fe_{2.5-x}Al_xO_4$, Fe^{3+} ions occupying B sites are replaced by Al^{3+} ions $[Fe_1^{3+}]_A[Li_{0.5}^{1+}Al_x^{3+}Fe_{1.5-x}^{3+}]_BO_4$. The magnetic moment in inverted ferrites is mainly caused by the resultant magnetic moment of the A and B sites. In ferrite-spinels, each ion in the A site has 12 ions in the B site as nearest neighbors, while an ion in the B site has 6 neighbors in the A site and 6 neighbors in the B site.
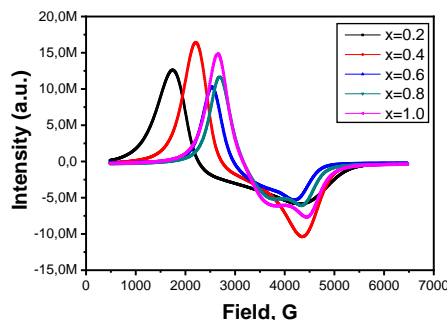

Fig. 3 – EPR spectra of a series of samples of the composition $Li_{0.5}Fe_{2.5-x}Al_xO_4$, where $x = 0.2$; 0.4; 0.6; 0.8; 1.0; synthesized by the sol-gel autocombustion method

According to Neel's model of the molecular field [33, 34], the A-B superexchange interaction is dominant over the A-A and B-B interactions. So, the magnetic moment per formula unit is given as $\mu = \mu_B - \mu_A$. Since we are replacing iron with a Al^{3+} non-magnetic ion in the B position, this leads to a decrease in the resulting magnetic moment in the ferrite $Li_{0.5}Fe_{2.5-x}Al_xO_4$.

Fig. 5 shows the dependence of saturation magnetization on temperature during heating and cooling from room temperature to 900 K.

As can be seen from the temperature behavior of saturation magnetization, with an increase in the content of aluminum ions in the system, the value of the Curie temperature increases, so, from Table 2, we can see that the lowest content of aluminum (system $x = 0.2$), the Curie temperature is 762 K, while the maximum value is acquired for a sample with $x = 0.8$ (801 K). Next, the value of the Curie temperature decreases slightly and for the sample with $x = 1.0$, it acquires a value of 787 K. This behavior of the systems is related to the fact that the presence of aluminum ions in the lattice increases the spin rotation energy.

The main magnetic parameters obtained from the remagnetization loops in the modes before and after heating are given in Table 2.

As can be seen from Table 2, when substituting iron with non-magnetic aluminum ions, the expected systematic decrease in magnetic parameters is not observed, which can be explained by the peculiarities of the structure and cation distribution. Accordingly, as mentioned earlier, the sample with substitution $x = 0.8$ is characterized by the maximum values of magnetic parameters, such as saturation magnetization, residual magnetization, and magnetic moment per formula unit. By comparing the data of Mössbauer spectroscopy and NMR experiments, this sample can be singled out as the one for which the A-B value of the interlattice interaction reaches the optimal value.
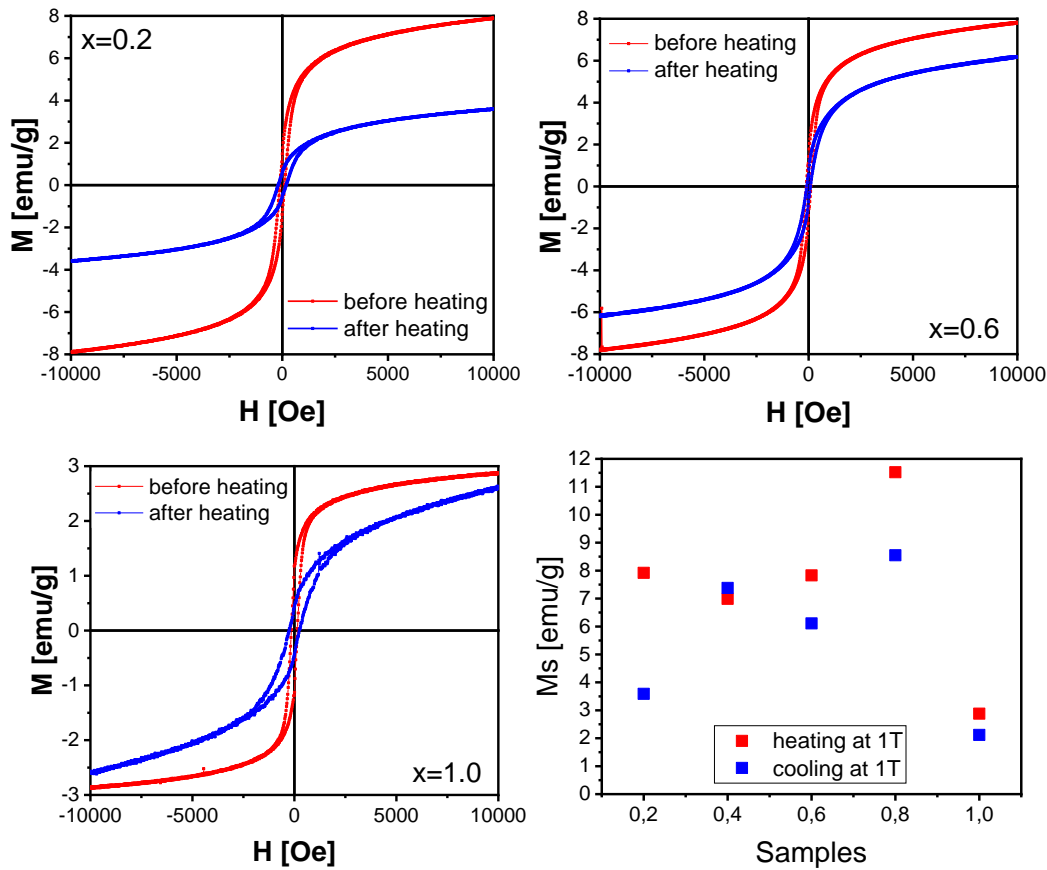
Fig. 4 – *M-H* curves and the change in the saturation magnetization of M_S with the composition of the system $Li_{0.5}Fe_{2.5-x}Al_xO_4$

Table 2 – The main magnetic parameters of aluminum-substituted lithium-iron spinels were obtained by the sol-gel auto-combustion method before and after heating to a temperature of 900 K

Aluminum content	Saturation magnetization, M_S Emu/g	Coercive power, H_C	Remanent magnetization, emu/g	Curie temperature, T_c, C	Magnetic moment per formula unit, m_e	Anisotropy constant, K 10^4	Molar mass, M
0.0	71.3	112	28.3	1020	2.63	0.83	207.10
0.2	7.92	111.8	1.35	762	0,285	2.34	201.27
0.4	6.99	104.8	1.38	786	0,245	2.13	195.49
0.6	7.83	108.5	1.28	797	0,266	2.14	189.72
0.8	11.52	166.7	2.97	801	0,379	3.19	183.95
1.0	2.88	146.3	1.17	787	0,092	2.72	178.17
Errors	±0,01	±0,1	±0,01	±1	±0,001	±0,01	±0,1

Optical studies of samples of the Li-Fe-Al system are represented by the Tauc plots in Fig. 6, which give a connection between the energy of the absorbed photon and the value of the band gap. The band gap (E_g) is related to the energy of the absorbed photon by the following relation

$$\alpha h\nu = A\,(h\nu - E_g)^n,$$

where α is the experimentally found absorption coefficient, hν is an energy of the absorbed photon, A is a constant that depends on the thickness of the cuvette, E_g is the width of the forbidden zone, and n is an exponent equal to 2 in the case of a direct transition of an excited electron from the valence band to the conduction band.

To determine the width of the band gap, finely ground ferrite powder was dissolved in double-distilled water and subjected to ultrasonic dispersion for 20 min. After that, the dependence of the transmission coefficient on the wavelength was obtained using a spectrophotometer. Based on these data, the dependence of ($\alpha h\nu$)^n on hν was built. By approximating the rectilinear section to zero, the optical band gap was obtained.

Fig. 6 shows the dependence of the band gap width on the composition.

As can be seen from the figure, a non-monotonic dependence of the optical band gap on the composition is observed. Moreover, the smallest values are observed for systems with values of $x = 0.0$ and 1.0. The largest value is for the sample with $x = 0.6$. Since the synthesized ferrites were characterized by a small value of crystallites [35] and fairly high values of the specific surface area [36], we checked their suitability for use as a photocatalyst for the degradation of the dye MB (methylene blue).
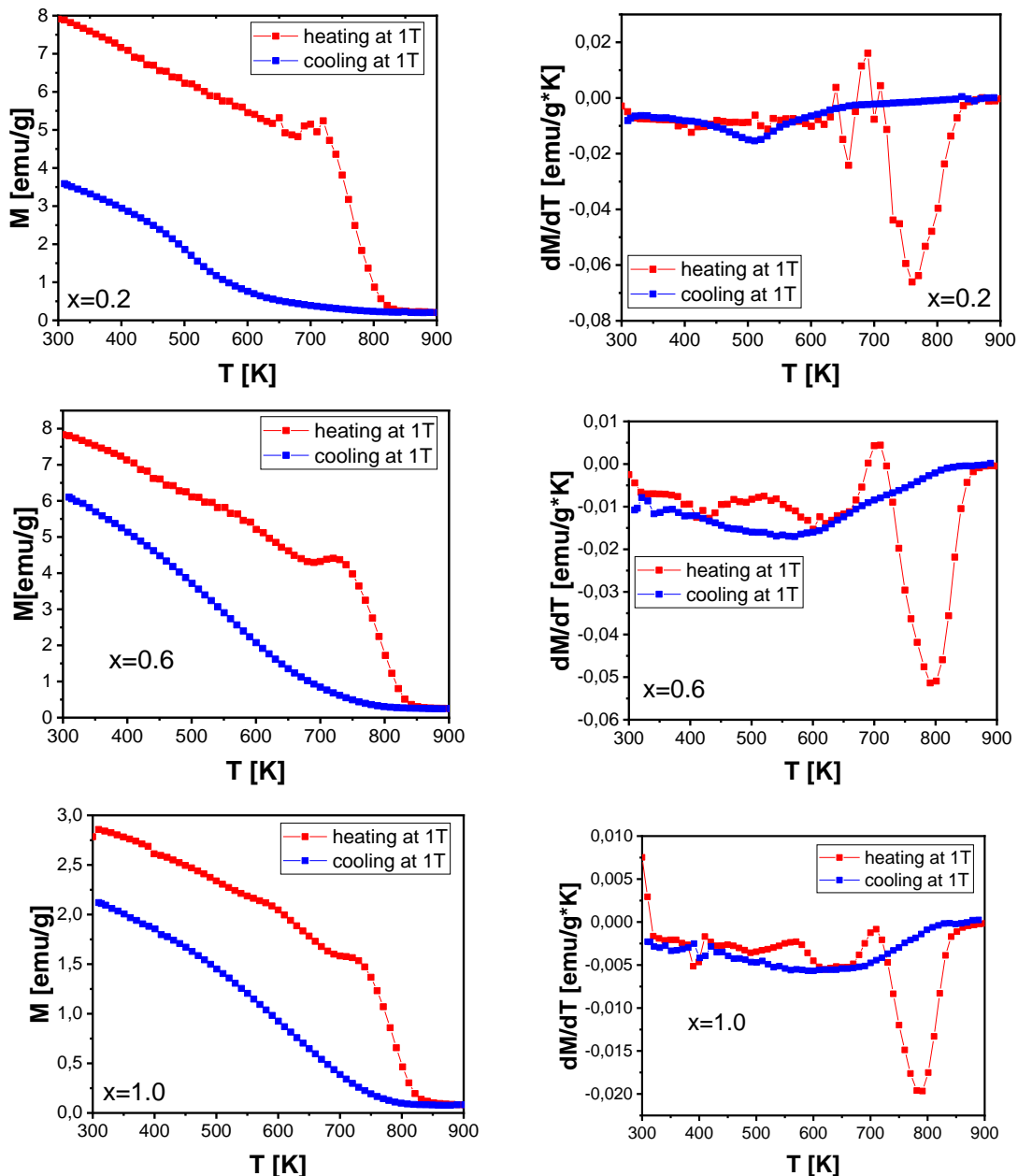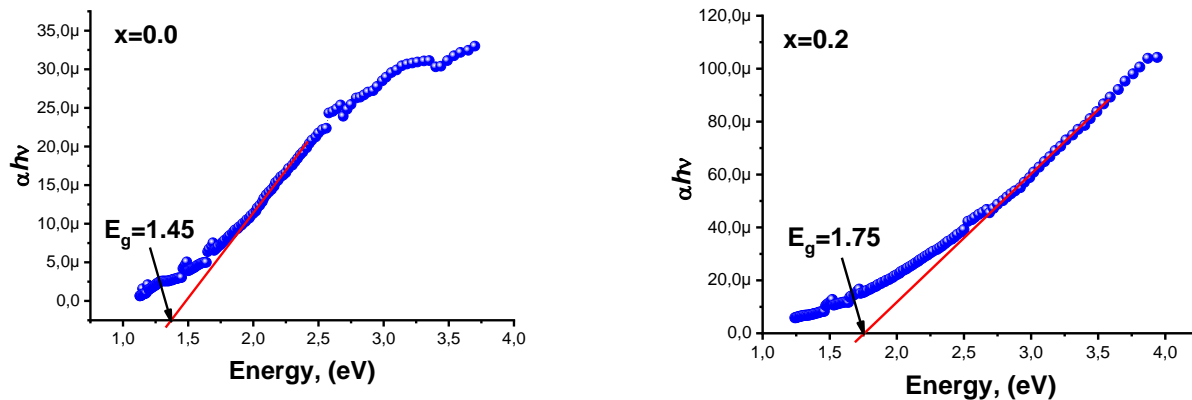
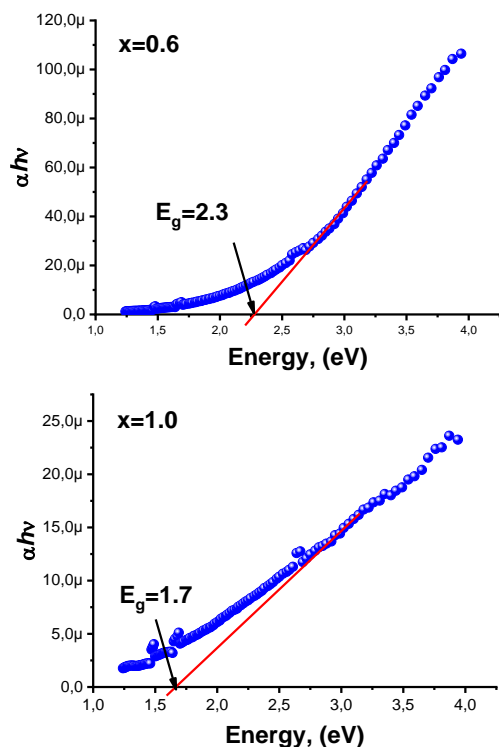**Fig. 5** – Dependence of saturation magnetization on temperature and its differential

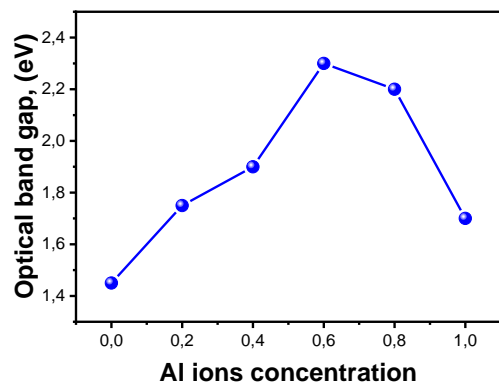**Fig. 6** – Tauc's plots for ferrite spinels with different contents of aluminum ions

Fig. 7 – Dependence of the gap width on the content of aluminum ions in ferrite

Fig. 8 shows the dependence of the change in dye concentration (C / C_0) on the irradiation time. As can be seen from the dependence, the system with the aluminum content $x = 0.0$ has the highest level of degradation, which in 140 min reaches a value of 98 %. Moreover, the dependence of the level of degradation (as well as the rate of degradation) in Fig. 9 during 120 min on the content of Al^{3+} ions is non-linear.

To determine the rate of degradation, the dependence of ln (C_0 / C) on the illumination time was plotted. A linear approximation of this dependence gave the rate of the degradation process. The dependence of ln (C_0 / C) on the illumination time is shown in Fig. 9.

The level of degradation was determined from the ratio $K = [1 - I / I_0] \cdot 100$ %. The change in the level of degradation depending on the time of illumination is shown in Fig. 10.
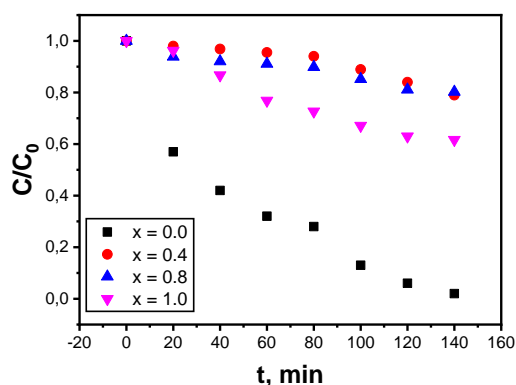

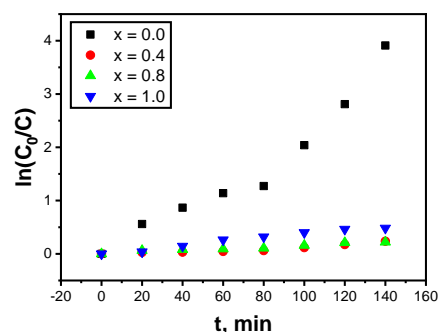**Fig. 8** – Dependence of the change in dye concentration on the illumination time

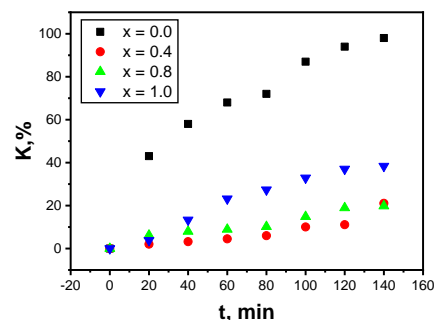**Fig. 9** – Dependence of Ln(C/Co) on illumination time.

Fig. 10 – Dependence of the level of degradation K on the illumination time

Table 3 shows the calculated values of the rate and level of degradation of methylene blue under the action of the photocatalyst based on the synthesized samples.

Table 3 – Degradation characteristics of the photocatalyst based on lithium-aluminum spinel

The composition of the photocatalyst	Degradation rate, min⁻¹	Degradation level, %
$Li_{0.5}Fe_{2.5}O_4$	0.0252	98
$Li_{0.5}Al_{0.4}Fe_{2.1}O_4$	0.0016	21
$Li_{0.5}Al_{0.8}Fe_{1.7}O_4$	0.0015	18
$Li_{0.5}Al_{1.0}Fe_{1.5}O_4$	0.0038	38

As can be seen from Figs. 8-10 and Table 3, there is a strong dependence of photocatalytic properties on the composition of ferrite. As is known, the main factors affecting degradation processes are the type and amount of substitution, the width of the band gap of the synthesized material, the cationic distribution of elements by sublattices, the area of the active surface,

etc. Fig. 11 shows the dependence of the maximum degree of degradation of methylene blue on the composition of ferrite acting as a photocatalyst.
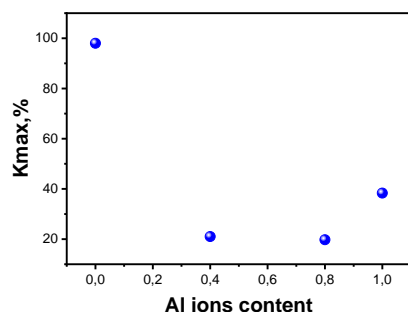

Fig. 11 – Dependence of the maximum level of dye degradation on the content of aluminum ions in the photocatalyst

As can be seen from the comparison of Fig. 7 and Fig. 11 there is an inverse relationship between the optical band gap and the maximum degradation ability of the studied compound as a photocatalyst. Thus, when the reaction mixture is illuminated with light of the visible range (halogen lamp with parameters), a higher rate and, accordingly, a higher level of degradation is observed for samples with a smaller value of the optical band gap

The magnetic nature of ferrite samples makes it possible to easily remove spent material from the water environment under the influence of an external magnetic field, which prevents the danger of contamination of the water environment with secondary compounds. In other words, the high magnetic properties of ferrite-based photocatalysts eliminate one of the important problems inherent in traditional compounds such as TiO_2, namely: they can be easily removed together with pollutants from the medium to be cleaned without the use of additional chemical or biological reagents.

4. CONCLUSIONS

Aluminum-substituted lithium-iron spinel of the general formula $Li_{0.5}Fe_{2.5-x}Al_xO_4$, synthesized by the sol-gel auto-combustion method, was studied by the methods of Mössbauer spectroscopy, NMR, and with the help of a sample vibration magnetometer. The research results showed that the main type of magnetic interaction in the studied ferrites is A-B interlattice interaction. The resulting magnetic moment of the system depends both on the content of the substitution element and on the selective entry into the A or B sublattice. The Al^{3+} and Li^+ cations mainly occupy the octahedral (B) positions, while the Fe^{3+} cations are distributed over both positions. The introduction of Al^{3+} in the B-position reduces the intensity of the IFNMR echo amplitude. Moreover, increasing the aluminum content reduces the value of the magnetic superexchange field and causes rapid growth of the paramagnetic component (doublet in Mössbauer spectra). A decrease in saturation magnetization leads to a decrease in signal intensity. The thermal additive reduces the observed echo signal. Our results showed that NMR and Mössbauer spectroscopy are complementary techniques for obtaining the magnetic properties of Li-Al ferrites in a wide range of frequencies. The synthesized ferrites were tested as photocatalysts for the removal of methylene blue from an aqueous medium. It is shown that the best degradation characteristics (level and rate of degradation) in the visible range of irradiation are possessed by those materials with a smaller width of the optical band gap.

REFERENCES

1. A.R. Chavan, V. Vinayak, S.M. Rathod, P.P. Khirade, *Physica B: Condens. Matter* **615**, 413075 (2021).
2. O.M. Uhorchuk, V.V. Uhorchuk, M.V. Karpets, M.I. Hasyuk, *J. Nano- Electron. Phys.* **7** No 2, 02012 (2015).
3. Y. Gao, Z. Wang, J. Pei, H. Zhang, *J. Alloy. Compd.* **774**, 1233 (2019).
4. L.S. Kaykan, J.S. Mazurenko, I.P. Yaremiy, Kh.V. Bandura, N.V. Ostapovych, *J. Nano- Electron. Phys.* **11** No 5, 05041 (2019).
5. Y. Guo, J. Zhu, H. Li, *Ceram. Int.* **47**, 9111 (2021).
6. B.K. Ostafiychuk, I.M. Gasyuk, L.S. Kaykan, V.V. Uhorchuk, P.P. Yakubovskiy, V.A. Tsap, Yu.S. Kaykan, *Metallofiz. Noveishie Tekhnol.* **36**, 89 (2014).
7. V. Rathod, A.V. Anupama, V.M. Jali, V.A. Hiremath, B. Sahoo, *Ceram. Int.* **43**, 14431 (2017).
8. L.S. Kaykan, J.S. Mazurenko, N.V. Ostapovych, A.K. Sijo, N.Ya. Ivanichok, *J. Nano- Electron. Phys.* **12** No 4, 04008 (2020).
9. M.V. Ushakov, V.D. Nithya, N. Rajeesh Kumar, S. Arunkumar, A.V. Chukin, R. Kalai Selvan, M.I. Oshtrakh, *J. Alloy. Compd.* **912**, 165125 (2022).
10. S.K. Jaiswal, R. Ranjan, J. Kumar, *J. Alloy. Compd.* **844**, 155832 (2020).
11. I. Soibam, S. Phanjoubam, C. Prakash, *J. Magn. Magn. Mat.* **321**, 2779 (2009).
12. C. Vidal-Abarca, P. Lavela, J.L. Tirado, *J. Power Source.* **196**, 6978 (2011).
13. L. Kaykan, A.K. Sijo, A. Żywczak, J. Mazurenko, K. Bandura, *Appl. Nanosci.* **10**, 4577 (2020).
14. M. Junaid, M.A. Khan, Z.M. Hashmi, G. Nasar, N.A. Kattan, A. Laref, *J. Molec. Struct.* **1221**, 128859 (2020).
15. A. Manzoor, M.A. Khan, M.Y. Khan, M.N. Akhtar, A. Hussain, *Ceram. Int.* **44**, 6321 (2018).
16. G. Aravind, M. Raghasudha, D. Ravinder, R.V. Kumar, *J. Magn. Magn. Mat.* **406**, 110 (2016).
17. L.S. Kaykan, A.K. Sijo, J.S. Mazurenko, A. Żywczak, *Appl. Nanosci.* **12**, 503 (2021).
18. L.S. Kaykan, J.S. Mazurenko, A.K. Sijo, V.I. Makovysyn, *Appl. Nanosci.* **10**, 2739 (2020).
19. I. Ahmad, T. Abbas, A.B. Ziya, A. Maqsood, *Cer. Int.* **40**, 7941 (2014).
20. A.V. Anupama, M. Manjunatha, V. Rathod, V.M. Jali, R. Damle, K.P. Ramesh, B. Sahoo, *J. Magn. Resonance* **286**, 68 (2018).
21. R.G. Kharabe, S.A. Jadhav, A.M. Shaikh, D.R. Patil, B.K. Chougule, *Mater. Chem. Phys.* **72**, 77 (2001).
22. M.M. Karanjkar, N.L. Tarwal, A.S. Vaigankar, P.S. Patil, *Ceram. Int.* **39**, 1757 (2013).

23. M.J. Iqbal, M.I. Haider, *Mater. Chem. Phys.* **140**, 42 (2013).
24. J.N. Pavan Kumar Chintala, S. Bharadwaj, M. Chaitanya Varma, G.S.V.R.K. Choudary, *J. Phys. Chem. Solid.* **160**, 110298 (2022).
25. C.A. Palacio Gómez, C.A. Barrero Meneses, J.A. Jaén, *J. Magn. Magn. Mat.* **505**, 166710 (2020).
26. G.P. Nethala, R. Tadi, G.R. Gajula, K.N. Chidambara Kumar, V. Veeraiah, *Physica B: Condens. Matter* **550**, 136 (2018).
27. *Physics in Biology and Medicine* (Elsevier: 2019).
28. K.P. Belov, *Phys.-Usp.* **39**, 623 (1996).
29. V.D. Doroshev, V.A. Klochan, N.M. Kovtun, V.N. Seleznev, *phys. status solidi a* **9**, 679 (1972).
30. G.M. Deikova, V.I. Greshnov, *Sov. Phys. J.* **13**, 1307 (1970).
31. S.S. Bellad, R.B. Pujar, B.K. Chougule, *Mater. Chem. Phys.* **52**, 166 (1998).
32. S.K. Nath, K.H. Maria, S. Noor, S.S. Sikder, S.M. Hoque, M.A. Hakim, *J. Magn. Magn. Mater.* **324**, 2116 (2012).
33. G. Mathubala, A. Manikandan, S. Arul Antony, P. Ramar, *J. Molec. Struct.* **1113**, 79 (2016).
34. A. Lakshman, P.S.V. Subba Rao, K.H. Rao, *Mater. Lett.* **60**, 7 (2006).
35. W.R. Agami, M.A. Ashmawy, A.A. Sattar, *J. Mater. Eng. Perform.* **23**, 604 (2013).
36. H. Zhao, Z. Zheng, K.W. Wong, S. Wang, B. Huang, D. Li, *Electrochem. Commun.* **9**, 2606 (2007).

Дослідження Li-Al феритів методами ядерного магнітного резонансу, UV спектроскопії і мессбауерівської спектроскопії

Ю. Мазуренко[1], Л. Кайкан[2], А. Żywczak[3], В. Коцюбинський[4], Х. Бандура[1], М. Мойсеєнко[1], А. Витвицький[1]

[1] *Івано-Франківський національний медичний університет, вул. Галицька 2, 76018 Івано-Франківськ, Україна*
[2] *Інститут металофізики ім. Г. В. Курдюмова НАН України, бульв. Акад. Вернадського, 36, 03142 Київ, Україна*
[3] *Academic Centre for Materials and Nanotechnology, AGH University of Science and Technology, Krakiw, Poland*
[4] *Прикарпатський національний університет імені Василя Стефаника, вулиця Шевченка, 57, 76018 Івано-Франківськ, Україна*

У роботі представлені результати досліджень літієвих феритів, заміщених іонами алюмінію методами ядерного магнітного резонансу (NMR), мессбауерівської спектроскопії та за допомогою вібраційного магнетометра зразків при кімнатній температурі. Результуючий магнітний момент системи залежить як від вмісту заміщуючого елементу, так і від селективного входження в А чи В підгратку. Катіони AL^{3+} і Li^+ переважно займають октаедричні (В) позиції, тоді як Fe^{3+} розподілений по обох позиціях. Впровадження Al^{3+} в В-позиції понижує інтенсивність IFNMR амплітуди ехо. Більше того, збільшення вмісту алюмінію зменшує значення магнітного надобмінного поля і спричиняє швидке зростання парамагнітної компоненти (дублет на мессбауерівських спектрах). Зменшення намагніченості насичення призводить до зменшення інтенсивності сигналу. Наші результати показали, що NMR і мессбауерівська спектроскопія є доповняльними методиками для опису магнітних властивостей Li-Al феритів в широкому околі частот. Дослідження деградації метилену синього у водному середовищі показали, що синтезований ферит здатний витупати як фотокаталізатор, що працює у видимому діапазоні освітлення. Показано, що оптична ширина забороненої зони і коефіцієнт деградації знаходяться в оберненій залежності

Ключові слова: Li ферити, ЯМР, Шпінель, Наночастинки, Магнітні властивості, Фотокаталіз.